DISTRIBUTION OF ALPHA PARTICLE TRACKS ON CR-39 DETECTOR IN RADON DIFFUSION CHAMBER

J.M. Stajic[1], V.M. Markovic[2], B. Milenkovic[1*], N. Stevanovic[2] and D. Nikezic[3]

[1]*University of Kragujevac, Institute for Information Technologies, Kragujevac, Department of Science, Jovana Cvijica bb, 34000 Kragujevac, Serbia*
[2]*University of Kragujevac, Faculty of Science, Kragujevac, Serbia*
[3] *The State University of Novi Pazar, Vuka Karadzica bb, 36300 Novi Pazar, Serbia*

ABSTRACT

The aim of this study was to investigate spatial distribution of alpha particle tracks produced by radon and its progeny in radon diffusion chambers. Three cylindrical chambers equipped with CR-39 detectors were used in the experiment. Radon concentration was estimated using RAD7 device. Distribution of alpha particle tracks on detector surface was found to be nonuniform; track density close to the chamber walls was up to 30% lower than in the centre. The results were compared with the predictions of analytical method applied to the same chamber dimensions. Critical angle of detection was expressed in relation to particle incident energy, using TRACK_VISION computer software. It was shown that the shape of track density distribution highly depends on the chamber size, as well as on the critical angle of particle detection. Sources of track density variation were investigated by analyzing partial contributions from volumetric and deposited fractions of radon and its progeny. Side-wall contribution increases while volumetric and plateout contributions decrease with increasing radial distance from detector center. Changing chamber dimensions affects the relative influences of these partial contributions, resulting in different distributions of visible tracks on detector surface. Experimental results were compared to the values obtained using previously developed software based on Monte Carlo method. Five different expressions of detector response function (V) were applied in the study; two of them significantly underestimated the experimental results.

Keywords: CR-39, radon, calibration coefficient, track density, critical angle

1. INTRODUCTION

Passive radon measurements are commonly performed by solid state nuclear track detectors (SSNTD) enclosed in diffusion chambers of arbitrary shape (usually cylindrical or conical), covered with filter papers or other membranes permeable to radon, but not to its progeny. ^{222}Rn gas diffuses into a chamber and decays in the chamber volume emitting alpha particles

* Corresponding author: B. Milenkovic, e-mail: bmilenkovic@kg.ac.rs

that can produce latent tracks in the detector material. In addition, radon progeny can deposit on the inner surfaces of the chamber. It is usually assumed that progeny atoms are uniformly distributed in the chamber volume as well as on the inner surfaces of the chamber. However, some researchers have suggested non-uniform progeny distribution (Palacios et al., 2005; Nikezic and Stevanovic, 2005; Stevanovic et al. 2017; Markovic et al., 2019). The progeny decay with relatively short half-lives, contributing to total alpha-track density on the detector. Studies have shown that the fraction of ^{218}Po that decays in a chamber air is less than 0.5, while ^{214}Pb and ^{214}Bi almost fully deposit before decaying (McLaughlin and Fitzgerald, 1994; Nikezic and Stevanovic, 2005, Koo et al., 2002, 2003). It is often assumed that thoron (^{220}Rn) cannot diffuse through membrane due to its short half-life and small diffusion length (Sasaki et al., 2006; Pressyanov 2008).

After the irradiation, nuclear track detectors are commonly subjected to chemical or electrochemical etching in order to make particle tracks visible. The density of tracks on detector surface is converted to radon concentration using calibration coefficient. Detector calibration can be performed by experimental (Abdalla and Hajry, 2015; Antovic et al., 2007; Ismail and Jaafar, 2011) or theoretical methods (Eappen et al., 2008; Palacios et al., 2008; Patiris et al., 2007; Sima, 2001). In the course of calibration, uniform distribution of tracks on SSNT detectors in radon diffusion chambers was usually assumed i.e. calibration coefficient is commonly taken as a constant. However, theoretical consideration has indicated that distribution of tracks can be nonuniform, depending on the size and shape of the chamber and detector, as well as, on the etching conditions applied (Nikezic and Stevanovic, 2005; Stevanovic et al. 2017; Markovic et al. 2019).

The aim of this study was to investigate distribution of alpha track density, as well as, calibration coefficients for circular CR-39 detectors exposed in radon diffusion chambers. The results obtained by experimental methods were compared with the results of previously developed analytical approach (Markovic et al, 2019) and Monte Carlo calculation (Nikezic et al., 2014) applied for three chamber dimensions used in the real experiment.

2. MATERIALS AND METHODS

2.1 Experiment

Three cylindrical cups covered by filter paper were used as radon diffusion chambers:
Chamber 1: radius R = 2 cm, height H = 3.5 cm;
Chamber 2: radius R = 3 cm, height H = 9 cm and
Chamber 3: radius R = 3.5 cm, height H = 6 cm.

Each chamber was supplied with a circular CR-39 detector (TASTRAK®, 1 mm thick) that covered the entire bottom of the chamber. Detectors were laser-engraved with concentric circles as shown in Fig.1. The distance between adjacent circles was 5 mm. Three chambers were placed in a hermetically sealed Plexiglas box (30 L in volume), along with a sample of uranium ore that was used as a radon source. Radon concentration inside of Plexiglas box was estimated using RAD7 radon monitor. Detectors were exposed for about 3 months (93 days). After that, chambers were opened, and CR-39 detectors were chemically etched for 5 h in 6.25 N solution of NaOH. The etching procedure was performed in a water bath at the

temperature of (70±1) ^{0}C. After the etching, the detectors were washed with distilled water in order to stop further etching.

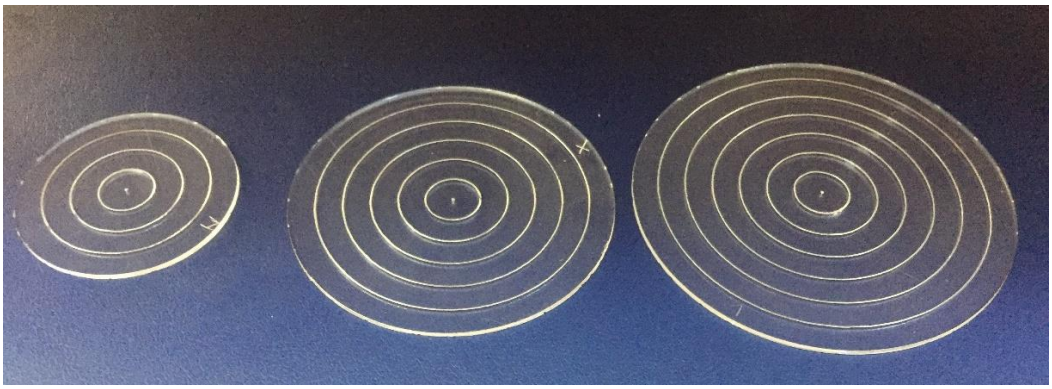

Figure 1. CR-3 detectors with engraved concentric circles and radii (from left to right) R_1=2 cm, R_2=3 cm and R_3= 3.5 cm placed in diffusion chambers 1, 2 and 3, respectively

Tracks were counted manually, using optical microscope. Track densities were estimated by randomly selecting about 50 visual fields at each circular stripe. The average track density obtained for each stripe was attributed to the corresponding radial distance from the centre of detector.

2.2 Analytical approach

Detail theoretical model of diffusion chamber was described by Markovic et al. 2019, where fundamental physical processes were used to describe track formation on the detector placed in a chamber. Model assumes cylindrical shape of diffusion chamber, enclosed with radon permeable filter paper. Diffusion of radon through filter paper into chamber is considered by assigning filter with diffusion coefficient D_1. It was assumed that pure air (without aerosols) was inside of chamber. Radon which diffuses through permeable filter paper has no ability to attach and deposit on chamber walls and its whole activity is distributed within the air volume of the chamber. Distribution of radon and its progeny volumetric activity concentrations is obtained by solving diffusion equation for radon diffusion through filter and air (Markovic et al. 2019):

$$\frac{\partial C_n(r,z,t)}{\partial t} = D \cdot \left(\frac{\partial^2 C_n(r,z,t)}{\partial r^2} + \frac{1}{r}\frac{\partial C_n(r,z,t)}{\partial r} + \frac{\partial^2 C_n(r,z,t)}{\partial z^2}\right) - \lambda_n \cdot C_n(r,z,t) + \lambda_{n-1} \cdot C_{n-1}(r,z,t) \quad (1)$$

where $n = 0,1,2,3$ denotes ^{222}Rn, ^{218}Po, ^{214}Pb and ^{214}Bi respectively, λ_n is decay constant of n_{th} progeny ($\lambda_{n-1} = 0$ for ^{222}Rn). Radon volumetric activities were found to be homogeneous in volume.

Next processes that govern behaviour of progeny in chamber are decay, diffusion and deposition. Diffusion equation of radon progeny takes into account source of their production

(which is decay of its precursor), diffusion inside of chamber volume and deposition onto chamber walls. Deposition of progeny onto chamber walls is taken into account by setting appropriate boundary conditions – zero concentration at the boundary (Pressyanov, 2008; Stevanovic et al, 2017; Markovic et al, 2019). Solving the set of diffusion equations for radon progeny, their volumetric activity concentrations were obtained. Calculating flux towards chamber walls enable determination of deposited activity rates, S_i. Another set of differential equations need to be solved to determine contributions of deposited progeny activities from decaying progeny precursors that are already deposited (Markovic et al, 2019):

$$\frac{dN_i}{dt} = S_i - \lambda_i N_i + \lambda_{i-1} N_{i-1}, \tag{2}$$

where $i = 1, 2, 3$ regards to ^{218}Po, ^{214}Pb and ^{214}Bi, and $\lambda_0 = 0$ since there are no deposited Rn atoms on the walls.

Following the above methodology, volumetric and deposited activities in diffusion chamber can be determined. Diffusion coefficients were taken as D_1=1.25·10^{-3} cm^2 s^{-1} for filter paper (Durcik and Havlik, 1996), and D_2=0.054 cm^2 s^{-1} for air inside the chambers (Nazaroff and Nero, 1988). The same diffusion coefficient was used for diffusion of radon and its progeny atoms inside the chambers. Diffusion coefficient in ambient air can vary for different progeny atoms since they tend to attach to aerosols (Amgarou, 2002). However, diffusion chambers covered with filter paper were assumed to be free of aerosols, and diffusion coefficients of progeny were taken as of the unattached atoms. In the literature, the range of 0.01 to 0.1 cm^2 s^{-1} was referenced for diffusion coefficients of radon and its unattached progeny atoms (Phillips et al, 1988; George and Knutson, 1994; Leonard, 1996; Knutson et al., 1997, Tokonami, 1999; Tymen et al., 1999; Malet et al, 2000; Amgarou, 2002). The mean value of 0.054 cm^2 s^{-1} was taken from Nazaroff and Nero (1988). The next step was to determine distribution of alpha particle track density on the detector which covers the whole area of the chamber bottom. This was done by summing contributions from decays of volumetric and deposited fractions for all progeny which emit alpha particles that can leave visible tracks on detector, Figure 2. Criteria for producing visible tracks on detector were introduced through range of alpha particles and critical angle (Markovic et al, 2019):

$$\begin{aligned} &\left[r_S \cos\varphi_S - r_D \cos\varphi_D\right]^2 + \left[r_S \sin\varphi_S - r_D \sin\varphi_D\right]^2 + \left[H - z_S\right]^2 \le \text{Range}^2 \\ &\left[r_S \cos\varphi_S - r_D \cos\varphi_D\right]^2 + \left[r_S \sin\varphi_S - r_D \sin\varphi_D\right]^2 \le \tan^2\frac{\theta}{2}\left[H - z_S\right]^2 \end{aligned} \tag{3}$$

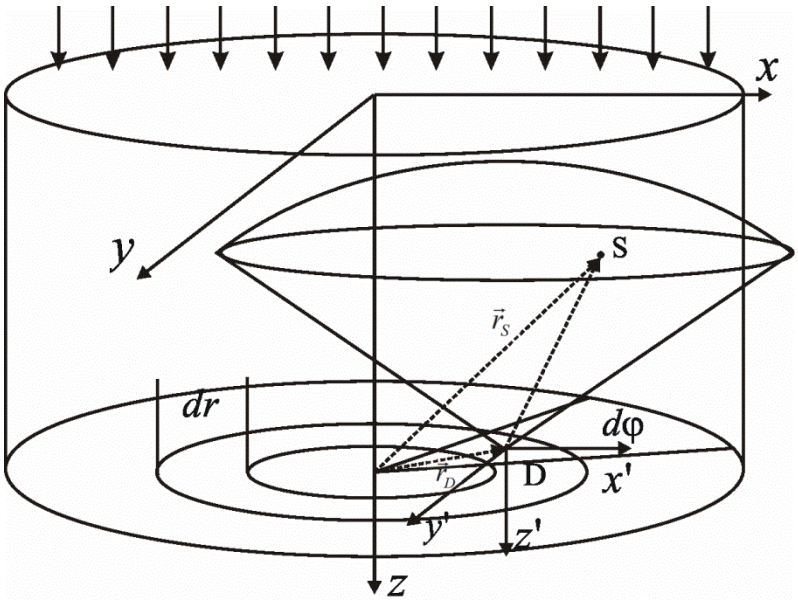

Figure 2. Schematic view of diffusion chamber. Upper arrows indicate direction of radon diffusion, O_{xyz} coordinate system is fixed for chamber cylinder, while $O_{x'y'z'}$ is coordinate system bound to detection point.

In Fig. 2, O_{xyz} origin is in the centre of filter, *z* axis is directed towards bottom of the chamber. Conditions given in Eq. 3 define ice-cream-shaped volume, formed as cross section of cone (with opening defined through critical angle) and sphere (with radius defined with range of alpha particles). Alpha particles emitted in this effective volume can contribute to tracks on detector. Summing up alpha particles emitted in effective volume, weighted according to the probability of hitting detector surface gives the total number of tracks that could be seen at the elementary surface of detector. Repeating this procedure for every elementary surface gives distribution of tracks on the detector (Markovic et al, 2019).

2.2.1 Critical angle of detection

Analytical method described above employs a function which relates critical angle of detection to particle incident energy. Five different functions were obtained using computer program TRACK_VISION (Nikezic and Yu, 2008). The program produces the optical appearances of alpha particle tracks in nuclear track materials based on incident energy, incident angle and removed layer during the etching. In addition to visualising particle tracks, the program also provides the parameters of track such as major and minor axes and track depths. In order to determine critical angle of detection, the program was executed for different alpha particle energies ranging from 0.01 MeV to 8.5 MeV while the incident angles were varied in the range of 1º – 90º with a step of 1º. Etching time (5 h) and bulk etch rate (1.06 μm h^{-1}) corresponding to the real experimental conditions were applied. The following five expressions for detector response function were implemented in the program:

$$V_1 = 1 + (11.45e^{-0.339R'} + 4e^{-0.044R'})(1 - e^{-0.58R'}) \text{ (Durrani and Bull,1987)} \quad (4)$$

$$V_2 = 1 + e^{-0.1R'+1} - e^{-R'+1.27} + e^{1.27} - e^{1} \text{ (Brun et al.,1999)} \quad (5)$$

$$V_3 = 1 + e^{-0.068R'+1.1784} - e^{-0.6513R'+1.1784} \text{ (Yu et al., 2005a)} \quad (6)$$

$$V_4 = 1 + e^{-0.06082R'+1.119} - e^{-0.8055R'+1.119}$$ (Yu et al., 2005b) (7)

$$V_5 = 1 + \frac{390}{(R'+2)^{2.35}} \cdot ln(R'+1) \cdot \left(1 - e^{-R'/5}\right) + \frac{R'}{80}$$ (Hermsdorf, 2009) (8)

where R' represents residual range of alpha particles in detector material.

Taking 1 μm of track diameter and depth as visibility criteria, critical detection angles in relation to particle incident energy (E) were obtained. Critical angles in respect to the normal to detector surface θ_{C1}, $\theta_{C2,}$…, and θ_{C5} (corresponding to the functions $V_{1,}$ V_2,…, and V_5, respectively) are presented in Figure 3. For given etching conditions, tracks were not developed for alpha particle energies below 0.1 MeV. Besides, when applying response functions V_3 and V_4, tracks produced by particles with energies above 7 MeV did not meet the visibility criteria even at normal incidence.

The data presented in Fig. 3 were well fitted with the function:

$$\theta_C(E) = \sum_{i=1}^{5} a_i \cdot E^{b_i} \cdot e^{-c_i E}$$ (9)

Fitting parameters a_i, b_i, and c_i (i = 1,2,3,4,5) are given in Table 1. Theoretical calculation of calibration coefficients took into account each of these functions and compared their prediction with the experimental results for each case.

Table 1. Fitting parameters for five functions of critical detection angle θ_{C1} – θ_{C5} corresponding to the response functions V_1 – V_5 (coefficient of determination R^2 for each fit is given in the last row)

	θ_{C1}	θ_{C2}	θ_{C3}	θ_{C4}	θ_{C5}
a_1	33.3630	9.4907e-3	30.9627	15.6977	10.5530
b_1	2.0951	-5.8437	1.5331	0.7533	0.6166
c_1	0.6444	3.4369	1.2099	0.2733	-4.0778e-3
a_2	37.0527	19.6300	3.5150	15.1462	0.6298
b_2	1.1380	0.3669	7.4133	0.7559	13.8183
c_2	1.5517	-0.0131	2.1386	0.2690	3.8767
a_3	158.2901	4.9021	18.5699	17.9516	17.7317
b_3	0.9874	1.3500	1.1808	0.7444	-0.5616
c_3	1.4660	1.0812	0.2808	0.2864	-0.0624
a_4	6.6378	243.9751	102.6803	18.2165	116.2258
b_4	2.1214	1.9326	1.5515	0.7281	2.1152
c_4	0.4321	2.2704	1.3261	0.2982	1.7099
a_5	-6.1985e-4	27.1464	-2.5945e-3	-0.0592	79.4112
b_5	-3.9621	3.0547	0.2571	1.9356	3.4437
c_5	-2.1277	1.0639	-1.2805	-0.3529	1.8776
R^2	**0.9982**	**0.9969**	**0.9996**	**0.9974**	**0.9798**

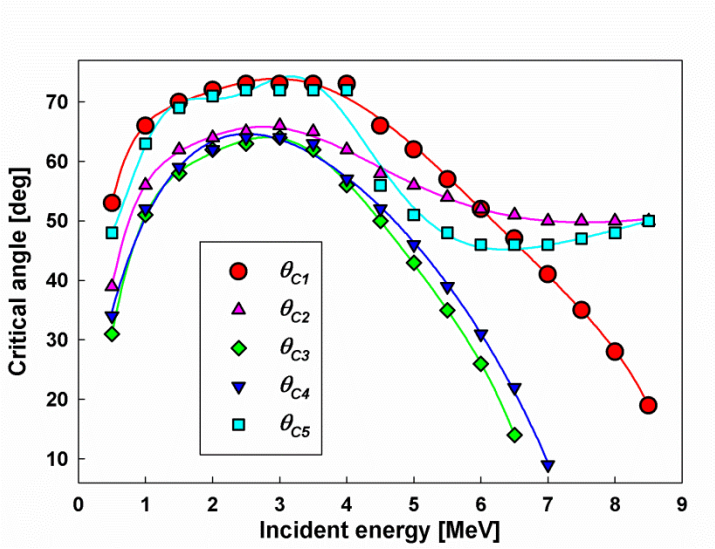

Figure 3. Critical detection angle as a function on particle incident energy (obtained by TRACK_VISION software)

2.2 Monte Carlo calculation

Fortran 90 computer program CR39_Sensitivity, previously developed by Nikezic et al. (2014) was also employed to estimate calibration coefficients for the chambers used in the experiment. The program calculates partial sensitivities of CR-39 detector for alpha particles emitted by radon and its progeny decayed in the chamber volume, deposited onto the chamber walls (and filter), and plated out on the detector itself. Total calibration coefficient is obtained by summing all of these contributions:

$$k_{MC} = k_0 + f_1 k_{1a} + (1 - f_1) k_{1w} + k_{4w} + (1 - f_1) k_{1p} + k_{4p} \qquad (10)$$

where f_1 is ^{218}Po volumetric fractions i.e. the fraction of ^{218}Po that decays in air before deposition (^{214}Po is assumed to decay as fully deposited); k_0 and k_{1a} are partial sensitivities to ^{222}Rn and ^{218}Po in chamber air, respectively; k_{1w} and k_{4w} are sensitivities to ^{218}Po and ^{214}Po deposited on chamber walls; k_{1p} and k_{4p} are sensitivities to ^{218}Po and ^{214}Po deposited on the detector (plateout) (Nikezic et al., 2014). The program assumes uniform deposition of radon progeny on the inner chamber surfaces (side walls, filter and detector).

The etching conditions as well as chamber dimensions applied in the experiment were used as input data for the program. The bulk etch rate was set to 1.06 μm h^{-1} (Stajic et al. 2018). The results were obtained for five V functions expressed by Eq. 4-8.

3. RESULTS AND DISCUSSION

3.1 Average radon concentration in calibration box

Figure 4 presents the build-up of radon concentration in the Plexiglas box, measured by RAD7 device. One-hour measurements were performed every 2 - 3 days during the first month of exposure.
The experimental data were fitted to the equation (Stajic et al., 2015):

$$C(t) = \alpha + \beta e^{-\gamma \cdot t} \tag{11}$$

where the parameters α, β and γ carry the information about three main processes that govern time evolution of radon activity concentration in the box: radon exhalation from the ore sample, radon decay and radon leakage from the box (back-diffusion processes can be neglected due to the small sample volume). Besides, α is obviously the equilibrium radon concentration ($t \to \infty$); $\alpha + \beta$ equals to the initial radon concentration in the box ($t = 0$) and γ is the sum of radon decay constant and radon leakage constant. Extrapolating the function (Eq. 11) to the exposure time of 93 days gives the average radon activity concentration in the box: $\bar{C}_{Rn} = (6.8 \pm 0.4)\ kBq\ m^{-3}$.

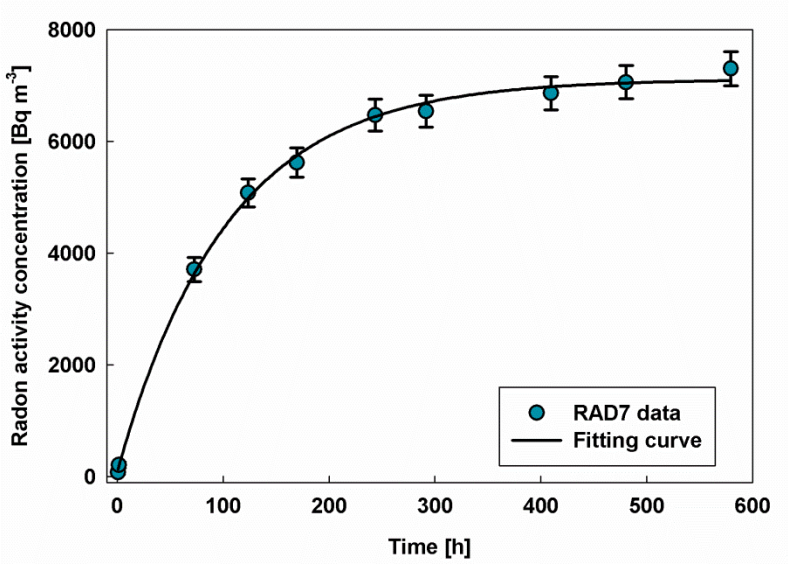

Figure 4. Build-up of radon activity concentration

Previous studies indicated that radon concentration inside diffusion chambers might be slightly lower than the outside value. A correction factor should be applied depending on chamber volume and filter properties such as thickness, surface area and radon diffusion coefficient (Amgarou, 2002). However, calculation of the correction factor for the current conditions indicated that the reduction of radon concentration was rather negligible for all three chambers and therefore it was assumed that the concentration inside of each chamber was equal to the value measured in the Plexiglas box.

3.2 Calibration Coefficient

It has been shown that distribution of alpha particle tracks on detector surface is not uniform. Track density was rather dependent on the distance from the centre i.e. it decreased by

approaching the side walls of each chamber (Figure 5). Experimental points were well-fitted by polynomial functions.

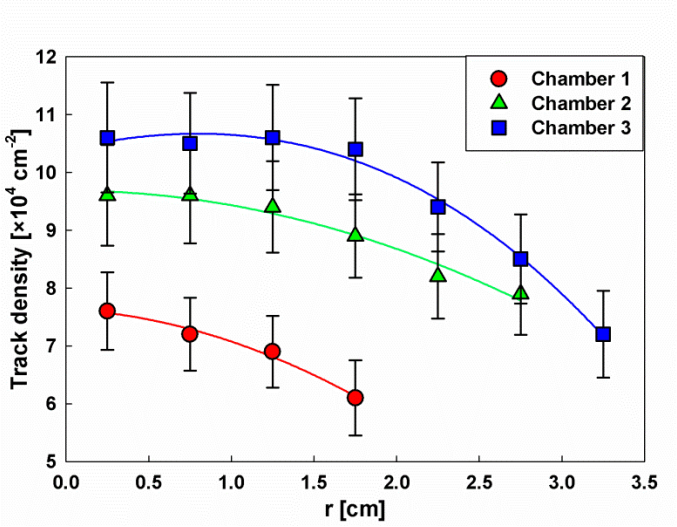

Figure 5. Alpha track density in relation to radial distance from the centre (obtained by experiment)

Assuming that average radon activity concentration in chambers was equal to the outside concentration ($\bar{C}_{Rn}$), average alpha track density (ρ_i) found on i^{th} circular stripe on detectors' surface was converted to calibration coefficient ($k_{EXP,i}$) using the relation:

$$k_{EXP,i} = \frac{\rho_i}{\bar{C}_{Rn} \cdot \Delta t} \tag{12}$$

where Δt represents the exposure time. Calibration coefficient $k_{EXP,i}$ as a function on radial distance from the centre of detector (which coincides with the centre of the chamber bottom) is presented in Figure 6 for the three chambers employed in the experiment. Depending on the chamber dimensions, calibration coefficient estimated close to the chamber walls was up to 30% lower than that in centre.

Figure 6 also presents the results of theoretical evaluation. Analytical calculation gave different values of calibration coefficients (k_{A1}, $k_{A2,}$…,k_{A5}) by applying five different functions for critical detection angle (θ_{C1}, $\theta_{C2,}$…,θ_{C5}, respectively). Analytical approach provided quite good agreement with the experimental results by applying the functions θ_{C1}, θ_{C2} and θ_{C5}. The best match was obtained for Chamber 2, but the analytical predictions obtained for Chambers 1 and 3 also fell within the experimental uncertainty ranges. Functions θ_{C1}, θ_{C2} and θ_{C5} gave quite similar results. Functions θ_{C3}, θ_{C4} underestimated the experimental values.

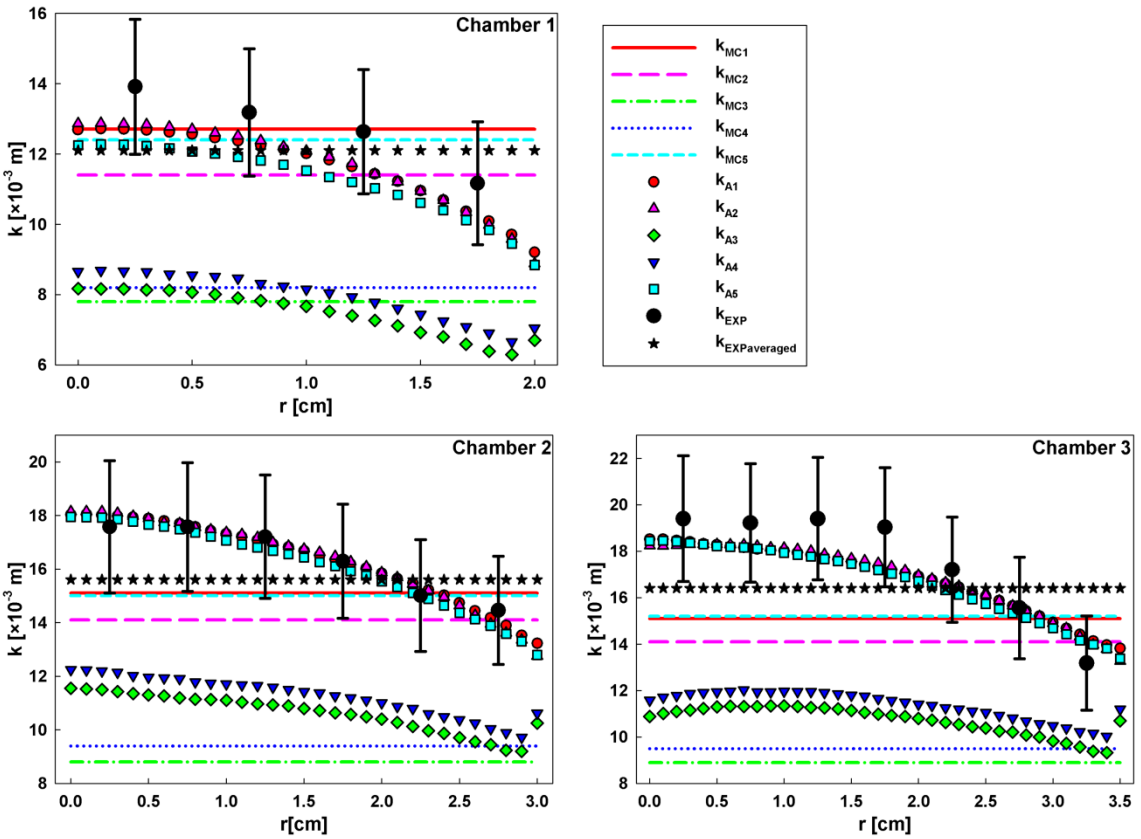

Figure 6. Calibration coefficients obtained by experiment (k_{EXP} and $k_{EXPaveraged}$), analytical method ($k_{A1} - k_{A5}$) and Monte Carlo approach ($k_{MC1} - k_{MC5}$)

Calibration coefficients k_{MC1}, $k_{MC2,...,}$ k_{MC5} obtained by applying computer program CR39_Sensitivity for five response functions (V_1 to V_5) are presented by straight lines in Figure 6. Although some authors suggested that ^{218}Po volumetric fraction was about 0.4 (Koo et al. 2003), McLaughlin and Fitzgerald (1994) obtained a lower value ($f_1 \rightarrow 0$) using Jacobi's model for the progeny in the diffusion chamber. The analytical model used in presented study gave the values of ^{218}Po volumetric fraction 0.02, 0.06 and 0.06 for in the chambers 1, 2 and 3, respectively. Therefore, these values were used as input parameters for CR39_Sensitivity program. Again, the functions V_1 and V_5 gave the best match to the experimental results which is in agreement with previous findings (Nikezic et al., 2014). Functions V_3 and V_4 underestimated the experimental values in all cases.

Experimental results confirmed the predictions of analytical model regarding non-uniform distribution of tracks on detector surface. However, averaging the track densities presented in Fig. 5 over the distance r (from $r = 0$ to $r = R$) gave the values: 6.62 $\times 10^4$ track cm^{-2}, 8.55 $\times 10^4$ track cm^{-2} and 8.94 $\times 10^4$ track cm^{-2} for chambers 1, 2 and 3, respectively. These values resulted in calibration coefficients presented by star symbols in Fig.6. Obviously, these values can still be quite well approximated by the results of Monte Carlo calculation (using response functions V_1 or V_5), particularly for chambers with smaller radius (1 and 2).

Theoretical model enables expanding exploration to different chamber sizes. Analysis was performed in order to investigate how radius of chamber affects the calibration

coefficient. Using analytical model, height of chamber was set to H=6 cm, and the radius was varied in the range from R=2 cm to R=6 cm. θ_{C1} function was chosen due to the best match to the experimental observations. Obtained calibration coefficient distributions are presented in Figure 7.

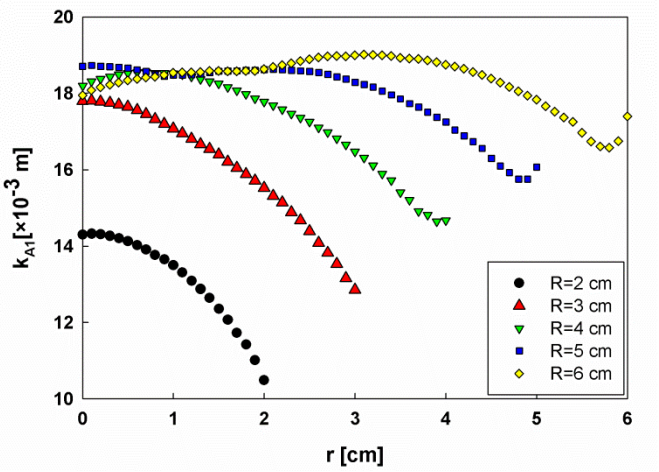

Figure 7. Calibration coefficient distributions for cylindrical diffusion chambers with height H=6 cm and different radii in the range from R=2 cm to R=6 cm.

It can be seen from the figure that distribution of calibration coefficient exhibits complex dependence on chamber radius. Depending on size of the chamber there can be up to 30% difference in calibration coefficient on different positions along radius. When chamber radius exceeds the range of alpha particles in air, there is no contribution from deposited fraction on the chamber cylinder wall to the tracks on the middle of the detector. In such cases, track density may increase with the distance from center. Complexity of calibration coefficient distribution is reflected through great number of different contributions to track density: tracks from ^{222}Rn, ^{218}Po and ^{214}Po alpha particles from volumetric activity; tracks from ^{218}Po and ^{214}Po alpha particles from deposited activity on chamber bottom (plateout), cylindrical wall and filter. Each of these partial activities has its own distribution which is related to chamber dimensions. Figure 8 shows all partial distributions for Chamber 2 used in this work, for critical angle θ_{C1}.

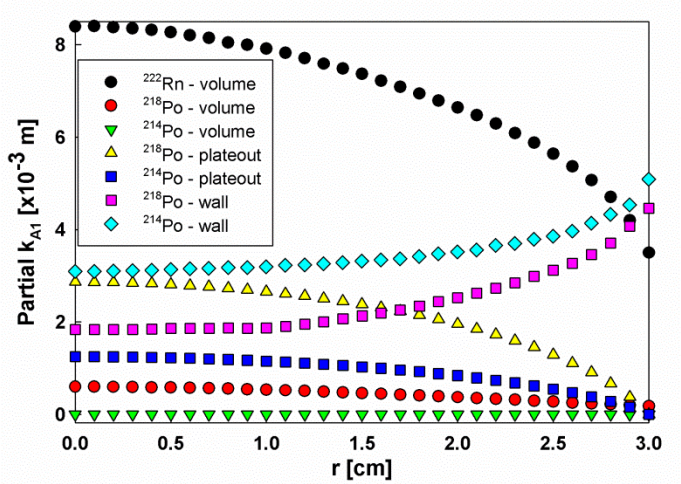

Figure 8. Partial calibration coefficients from radon and progeny volumetric and deposited fractions. Fraction from filter wall in not included in figure 7 since height of chamber exceeds range of alpha particle, and there is no contribution from these fractions.

Figure 8 gives insight in track density distributions and calibration coefficient. In this case, there is no contribution from filter, due to large height of the chamber. Main contribution in the center of the detector is from ^{222}Rn volumetric fraction, approximately 50%. ^{214}Po volumetric fraction has negligible influence on track density, while ^{218}Po contribute with only about 5%. Bottom and cylinder wall fraction from ^{218}Po and ^{214}Po have contribution up to 50%. Contributions of partial fractions change along radius; deposited fractions have main contribution near the side walls. On the other hand, plateout and volumetric contributions decrease with increasing radial distance from detector center due to the fact that points in the middle of detector are exposed from all sides (i.e 2π sr irradiation geometry), while the points close to the chamber walls are exposed only from one side.

Conclusion

Non-uniform distribution of alpha particle tracks on detector surface was confirmed by experimental methods. Track density observed in the experiment decreased with increasing the distance from the centre. Experimental results are in good agreement with the predictions of analytical method. Shape of track density distribution depends on radius and height of the chamber and critical angle of alpha particles that form visible tracks. "Local" calibration coefficients can vary considerably when estimated in different areas of detector surface; distribution of calibration coefficient exhibits complex dependence on chamber dimensions due to different contributions of volumetric and deposited fractions of alpha-particle-emitting radionuclides. Chamber shape and dimensions affect the distribution of deposited radon progeny on the chamber surfaces and also their ability to produce visible tracks in detector. The contribution of volumetric fraction of radon and its progeny to track density is also not uniform. Treating calibration coefficient as a constant is usually justified for small surface area detectors. However, theoretical consideration shows that even in those cases, a variation of track density can be expected depending on the chamber radius and height.

Distribution of tracks on detector surface can be different in each particular case and cannot be readily predicted. This fact might have certain impact on the practical application of radon diffusion chambers in radon measurements. It is recommended to use detectors with radius less than 30% of the chamber radius and also to ensure the uniformity of track counting during the calibration and measurements in order to minimize possible errors. In the case of relatively large area detectors, a random selection of limited number of visual fields during track counting might result in overestimation or underestimation of average track density inducing an additional uncertainty in determining the calibration coefficient or radon activity concentration.

Five different V functions were used in the calculation part of this work. Three of them are in relatively good agreement among themselves as well as with the experimental data, while other two (functions V_3 and V_4) are in disagreement. These two functions were obtained differently from the others; function V_3 was determined by measurement of track

depth using atomic force microscope, while function V_4 was estimated through the height of track replicas in convenient material. The reason for the discrepancy is not known and it could be the subject of some further investigation.

Acknowledgement

The present work was supported by the Ministry of Education, Science and Technological Development of the Republic of Serbia (171021, 451-03-68/2020-14/200378).

References

Abdalla, A.M., Hajry, A.A., 2015. Radon irradiation chamber and its applications. Nucl. Instrum. Methods Phys. Res. 786, 78–82.

Amgarou K., 2002. Long-Term Measurements of Indoor Radon and its Progeny in the Presence of Thoron Using Nuclear Track Detectors: A Novel Approach. PhD Thesis, available at https://ddd.uab.cat/record/37276?ln=en .

Antovic, N., Vukotic P., Zekic, R., Svrkota, R., Ilic, R., 2007. Indoor radon concentrations in urban settlements on the Montenegrin Coast. Radiat. Meas. 42, 1573–1579.

Brun, C., Fromm, M., Jouffroy, M., Meyer, P., Groetz, J.E., Abel, F., Chambaudet, A., Dorschel, B., Hermsdorf, D., Bretschneider, R., Kadner, K., Kuhne, H., 1999. Intercomparative study of the detection characteristics of the CR-39 SSNTD for light ions: present status of the Besancon-Dresden approaches. Radiat. Meas. 31, 89–98.

Durrani, S.A., Bull, R.K., 1987. Solid State Nuclear Track Detection. Principles Methods and Applications. Pergamon Press.

Durcik, M., Havlik, F., 1996. Experimental study of radon and thoron diffusion through barriers. J. Radiat. Nuc. Chem. 209, 307–313.

Eappen, K.P., Sahoo, B.K., Ramachandran, T.V., Mayya, Y.S., 2008. Calibration factor for thoron estimation in cup dosimeter. Radiat. Meas. 43, S418–S421.

George A. C. and Knutson E. O., 1994. Particle size of unattached radon progeny in filtered room air. Radiat. Prot. Dosim. 56, 119-121.

Hermsdorf, D., 2009. Evaluation of the sensitivity function V for registration of α-particles in PADC CR-39 solid state nuclear track detector material. Radiat. Meas. 44, 283–288.

Ismail, A.H., Jaafar, M.S., 2011. Design and construct optimum dosimeter to detect airborne radon and thoron gas: Experimental study. Nucl. Instrum. Meth. Phys. Res. B 269, 437–439.

Knutson E. O., George A. C., Tu K. W., 1997. The graded screen technique for measuring the diffusion coefficient of radon decay products. Aerosol Sci. Technol. 27, 604-624.

Koo, V.S.Y., Yip, C.W.Y., Ho, J.P.Y., Nikezic, D., Yu, K.N., 2002. Experimental study of track density distribution on LR115 detector and deposition fraction of ^{218}Po in diffusion chamber. Nucl. Instr. Meth. Phys. Res. A 491, 470–473.

Koo, V.S.Y., Yip, C.W.Y., Ho, J.P.Y., Nikezic, D., Yu, K.N., 2003. Deposition fractions of ^{218}Po in diffusion chambers. Appl. Radiat. Isot. 59, 49–52.

Leonard B. E., 1996. High ^{222}Rn levels, enhanced surface deposition, increased diffusion coefficient, humidity, and air exchange effects. Health Phys. 70, 372-387.

Malet J., Michielsen N., Boulaud D., Renoux A., 2000. Mass transfer of diffusive species with non constant in-flight formation and removal in laminar tube flow: application to unattached short-lived radon daughters. Aerosol Sci. Technol. 32, 168-183.

Markovic, V.M., Markovic, A.G., Stevanovic, N., Nikezic, D., 2019. Rn progeny diffusion, deposition and track distribution in diffusion chamber with permeable membrane. Radiat. Meas. 124, 146–157.

McLaughlin, J.P., Fitzgerald, B., 1994. Models for determining the response of passive alpha particle detectors to radon and its progeny in cylindrical detecting volumes. Radiat. Prot. Dosim. 56, 241–246.

Nazaroff W.W., Nero A.V., 1988, Radon and its decay products in indoor air. John Wiley & Sons

Nikezic, D., Stevanovic, N., 2005. Radon progeny behavior in diffusion chamber, Nucl. Instrum. Methods Phys. Res. B 239, 399–406.

Nikezic, D., Yu, K.N., 2008. Computer program TRACK_VISION for simulating optical appearance of etched tracks in CR-39 nuclear track detectors. Comput. Phys. Commun. 178, 591–595.

Nikezic, D., Yu, K.N., Stajic, J.M., 2014. Computer program for the sensitivity calculation of a CR-39 detector in a diffusion chamber for radon measurements. Rev. Sci. Instrum. 85 022102.

Palacios, D., Sajo-Bohus, L., Greaves, E.D., 2005. Radon progenydistributions inside a diffusion chamber and their contributions to track density in SSNT detectors. Radiat. Meas. 40, 657–661.

Palacios, D., Palacios, F., Sajo-Bohus, L., Barros, H., Greaves, E. D., 2008. LR-115 detector response to ^{222}Rn, ^{220}Rn and their progenies, exposed to hemispherical surfaces in free air, and design of a system to calculate their concentrations. Radiat. Meas. 43, S435–S439.

Patiris, D.L., Blekas, K., Ionnides, K.G., 2007. TRIAC II. A MatLab code for track measurements from SSNT detectors. Comput. Phys. Commun. 177, 329–338.

Phillips C. R., Khan A. and Leung H. M. Y., 1988. The nature and determination of the unattached fraction of radon and thoron progeny. in: Radon and its decay products in indoor air, eds. Nazaroff W. W and Nero A. V., John Wiley & Sons, pp. 203-256.

Pressyanov, D., 2008. Radon progeny distribution in cylindrical diffusion chambers. Nucl. Instrum. Methods Phys. Res. 596, 446–450.

Sasaki, T., Gunji, Y., Okuda, T., 2006. Transient-diffusion measurement of Radon in Japanese soils from a mathematical viewpoint. J. Nucl. Sci. Technol. 43, 806–810.

Sima, O., 2001. Monte Carlo simulation of radon SSNT detectors. Radiat. Meas. 34, 181–186.

Stajic, J.M., Milenkovic, B., Nikezic, D., 2015. Radon concentrations in schools and kindergartens in Kragujevac city, Central Serbia. CLEAN – Soil, Air, Water, 43, 1361–1365.

Stajic, J.M., Milenkovic, B, Nikezic, D., 2018. Study of CR-39 and Makrofol efficiency for radon measurements. Radiat. Meas. 117, 19–23.

Stevanovic, N., Markovic, V.M., Nikezic, D., 2017. Time dependence of ^{222}Rn, ^{220}Rn and their progeny distributions in a diffusion chamber. Nucl. Instrum. Methods Phys. Res. A 872, 93–99.

Tokonami S., 1999. Determination of the diffusion coefficient of unattached radon progeny with a graded screen array at the EML environmental chamber. Radiat. Prot. Dosim. 81, 285-290.

Tymen G., Kerouanton D., Huet C., Boulaud D., 1999. An annular diffusion channel equipped with a track detector film for long-term measurements of activity concentration and size distribution of nanometer ^{218}Po particles. J. Aerosol Sci. 30, 205-216.

Yu, K.N., Ho, J.P.Y., Nikezic, D., Yip, C.W.Y., 2005a. Determination of the V Function for CR-39 by Atomic Force Microscope. In Recent Advances in Multidisciplinary Applied Physics. Elsevier, Amsterdam, pp. 29–34.

Yu, K.N., Ng, F.M.F., Nikezic, D., 2005b. Measuring depths of sub-micron tracks in a CR-39 detector from replicas using atomic force microscopy. Radiat. Meas. 40, 380–383.